

Trapping and Imaging Single Dysprosium Atoms in Optical Tweezer Arrays

Damien Bloch,^{*} Britton Hofer, Sam R. Cohen,[‡] Antoine Browaeys, and Igor Ferrier-Barbut[♯]
Université Paris-Saclay, Institut d'Optique Graduate School, CNRS, Laboratoire Charles Fabry, 91127, Palaiseau, France

 (Received 17 July 2023; accepted 26 September 2023; published 14 November 2023)

We report the preparation and observation of single atoms of dysprosium in arrays of optical tweezers with a wavelength of 532 nm, imaged on the intercombination line at 626 nm. We use the anisotropic light shift specific to lanthanides and in particular a large difference in tensor and vector polarizabilities between the ground and excited states to tune the differential light shift and produce tweezers in near-magic or magic polarization. This allows us to find a regime where single atoms can be trapped and imaged. Using the tweezer array toolbox to manipulate lanthanides will open new research directions for quantum physics studies by taking advantage of their rich spectrum, large spin, and magnetic dipole moment.

DOI: 10.1103/PhysRevLett.131.203401

Trapping and cooling of single atoms in tweezer arrays [1,2] has allowed tremendous progress in quantum science and metrology [3,4]. These techniques were first used on alkali atoms [5–7], before being extended to alkaline-earth species [8–10] and molecules [11]. In parallel to this progress, experiments with quantum gases of lanthanides have explored dipolar physics [12] and topology [13,14] among other examples. Controlling lanthanides in single-atom tweezers will offer new possibilities for exploiting their specific properties. Their anisotropic light-matter interaction [15,16] results in a broad tunability of trapping potentials useful to produce subwavelength interatomic distances [17,18] or for quantum-enhanced sensing [19]. Dimers with a large magnetic dipole moment [20,21] or atoms with an electric dipole [22,23] might be produced to study quantum magnetism [24] in tweezer arrays. Finally, their many transitions from the ground state, spanning a broad range of wavelengths and linewidths makes them an interesting platform for studies of collective light-matter interactions [25–27]. In this Letter, we demonstrate single-atom trapping of dysprosium in optical tweezers, imaging on the narrow intercombination line by making use of the strong anisotropic light shift of Dy.

The rich spectrum of optical transitions of lanthanides has been used to operate efficient laser cooling and produce degenerate quantum gases [12]. Transitions from the $6s^2$ electrons are similar to those of two-electron atoms such as Yb and Sr, and the methods developed to prepare single atoms of these species can be adapted to lanthanides. Here, we rely on the intercombination line between $G = 4f^{10}6s^2I_8$ and $E = 4f^{10}(^5I_8)6s6p(^3P_1)(8, 1)_9$ of Dy, generally used for magneto-optical traps [28,29], to image single Dy atoms. This transition has a wavelength $\lambda = 626$ nm and a linewidth $\Gamma = 2\pi \times 135$ kHz. Another advantage of lanthanides is their nonvanishing vector and tensor polarizabilities. The tensor polarizability was

recently used to demonstrate magic trapping for the Dy intercombination transition at a trap wavelength of 1070 nm [16]. We rely in this work both on the tensor and vector polarizabilities [30] to obtain magic trapping at 532 nm.

We generate 5×5 tweezer arrays with 5 μm spacing at a wavelength of 532 nm [31] using a 2D acousto-optic deflector (AOD) driven by a multitone signal [6,32]. The tweezer light is sent through a 0.5-numerical aperture (NA) microscope objective (Mitutoyo G Plan Apo 50X) placed outside a glass cell, resulting in a tweezer waist $w_0 \approx 500$ nm [35]. Each trap has a power of 2 mW, yielding a potential depth of about 150 μK . Our setup is schematized in Fig. 1(a) and more details will be published in [36]. We use the ^{162}Dy isotope in this work. The experiment begins with a 2D magneto-optical trap (MOT) on the broad transition of Dy at 421 nm, as in [37], to cool and redirect atoms toward a glass cell. In the glass cell, we capture the atoms with a two color core-shell MOT [38] and eventually transfer them to a MOT using only the narrow intercombination line. Following the MOT loading stage, the atoms are pumped in the lowest Zeeman state $|g\rangle = |G, J = 8, m_J = -8\rangle$ by ramping the intensity to $I = 0.1I_{\text{sat}}$, with $I_{\text{sat}} = 72 \mu\text{W}/\text{cm}^2$, and detuning to $\Delta = -(2\pi)1.5$ MHz [28,29]. The tweezers are overlapped for 100 ms on the MOT. After this, each trap is filled with more than one atom on average.

Dysprosium has a large Zeeman manifold in both the ground state ($J = 8$) and excited state ($J' = 9$). This strongly influences imaging and cooling since the scattering rate on a narrow transition depends on the atom's internal state. We apply a magnetic field of 7 G to isolate a closed σ^- transition between $|g\rangle$ and $|e\rangle = |E, J' = 9, m'_J = -9\rangle$. This leaves the π ($m_J = -8 \leftrightarrow m'_J = -8$) and σ^+ ($m_J = -8 \leftrightarrow m'_J = -7$) transitions strongly off-resonance, respectively detuned by about 13 and 25 MHz (95 and

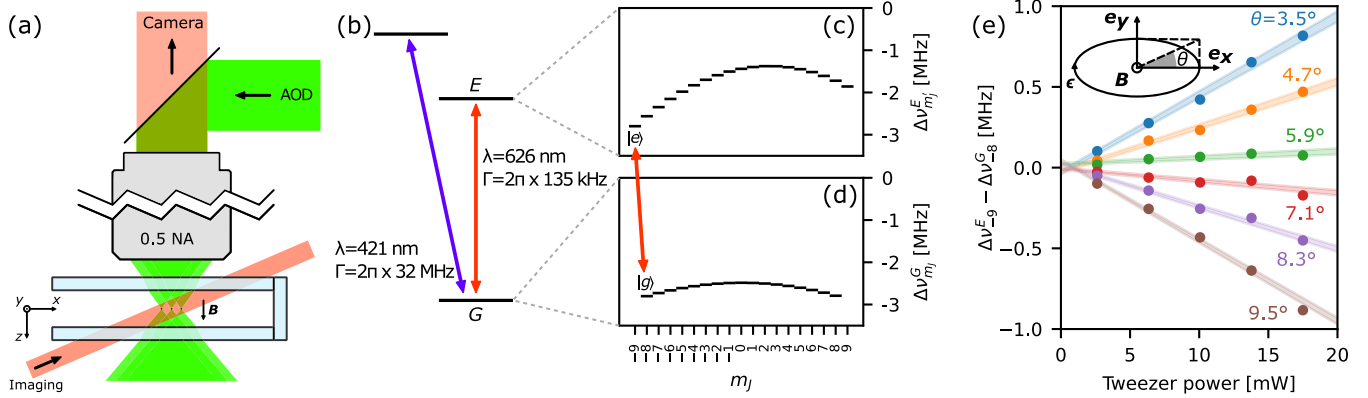


FIG. 1. (a) Simplified diagram of the beams used to trap and image single atoms in the tweezers. MOT beams are not shown here. (b) Relevant energy levels of Dy and their associated optical transitions used in this work. (c) Anisotropic light shift experienced by the Zeeman states in both the ground $\Delta\nu_{m_j}^G$ and (d) excited $\Delta\nu_{m_j}^E$ manifolds in magic conditions. The values plotted here are obtained by diagonalizing the full Hamiltonian including the Zeeman effect and the trap light shift. We then subtract the Zeeman shift to the eigenvalues of the Hamiltonian, to keep only the light shift. (e) Measured frequency difference between $|g\rangle$ and $|e\rangle$ with respect to their unperturbed frequency as a function of tweezer power and for different ellipticities θ of the tweezer polarization; shaded areas are linear fits with confidence interval.

190 Γ , respectively). It ensures negligible photon scattering rates for these transitions and the atoms are then imaged solely on the cycling σ^- transition.

To obtain single atoms we induce light-assisted collisions that eject pairs of atoms from the multiply-loaded tweezers [1]. We observe that such collisions take place in a few milliseconds when shining red-detuned light. The collision pulse lasts for 10 ms and has the same parameters as used for imaging specified below. After this, the tweezers are randomly loaded with zero or one atom, with a filling fraction close to 50%.

Next, to image single atoms, we need to precisely tune the trapping potential. Indeed for such a narrow linewidth, high fidelity single-atom imaging requires magic trapping where $|g\rangle$ and $|e\rangle$ have the same polarizability [10,39]. Whether or not such a condition exists for a given species depends in general on the trapping wavelength. In contrast with other species, the strong anisotropy of the polarizability of lanthanides allows one to tune the differential polarizability between $|g\rangle$ and $|e\rangle$ by changing the tweezer polarization [15,16]. This can lead to magic trapping in broad ranges of wavelengths. Measurements of the scalar, vector, and tensor polarizabilities for both the ground (G) and excited (E) manifolds at 532 nm will be reported in [36]. We use the large vector polarizability of the excited state and create an elliptic polarization of the tweezers, with Jones vector $(\epsilon_x, \epsilon_y) = (\cos\theta, i\sin\theta)$ in the plane perpendicular to the magnetic field. Figure 1(e) shows the shift of the transition measured with fluorescence spectroscopy as a function of trap power for different ellipticities θ . We find an ellipticity $\theta \simeq +6^\circ$ for which the transition $|g\rangle \leftrightarrow |e\rangle$ is magic [see Figs. 1(c) and 1(d)].

This magic trapping condition allows us to image single atoms in the tweezers. Fluorescence is induced by a single

nonretroreflected beam with propagation axis having components along both the radial and axial directions of the tweezers [10], which is necessary to cool efficiently while imaging. This beam is red-detuned by $\Delta = -1.0 \Gamma$ and has an intensity $I = 0.8I_{\text{sat}}$. The duration of the imaging pulse is typically 30 ms. The light scattered by the atoms is collected onto a CMOS camera (Hamamatsu C15550-20UP) through the same microscope objective used to focus the traps. For a single shot image as in Fig. 2(a), we count the number of collected photons in a small circular area around each trap. We repeat the experiment, reloading the MOT and the tweezers for every shot, and we record the histogram of the collected fluorescence as shown in Fig. 2(c). The histograms exhibit two peaks characteristic of the single-atom regime: one peak corresponding to zero atoms and the other peak, with about 50 photons detected, corresponding to a single atom in the trap.

These histograms are shifted and broadened by background light. This light is due to the tweezers beam at 532 nm going through the microscope and causing the glass of the lenses inside the objective to fluoresce at longer wavelengths, including the imaging wavelength of 626 nm. To mitigate this effect, two angle-tunable dichroic filters, one short-pass and one long-pass (Semrock TSP01-628 and TLP01-628), are placed on the path before the camera to transmit only a narrow wavelength band around 626 nm. This reduces the light reaching the camera to about 20 photons per pixel per second for 50 mW of 532 nm light going through the microscope. This remaining background can be seen in Fig. 2(b).

To determine the presence of a single atom in a given picture, we compare the number of photons collected to a given threshold. If the fluorescence is higher than the threshold, we label the trap as containing an atom,

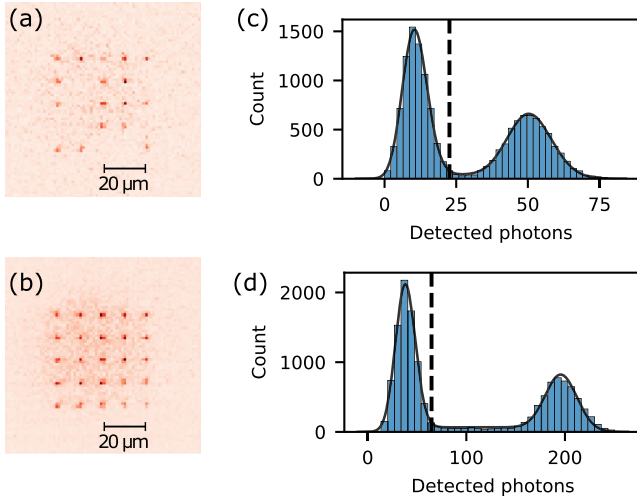


FIG. 2. (a) Single shot and (b) average picture of 5×5 trap arrays for exposure time of 30 ms. The halo that can be seen between traps on the average image is due to the fluorescence of the microscope objective. (c) Histogram of the fluorescence of the central trap for 30 ms (d) and 100 ms exposure time. The line is a fit to the sum of two peak distributions joined by a “bridge” (see text). Dashed lines indicate the chosen threshold to maximize the imaging fidelity F .

otherwise we label it as empty. In the following, we characterize the fidelity and induced losses of our imaging. The fidelity represents the probability to correctly label the *initial* presence of an atom in a trap. In addition, losses might be induced by the imaging sequence through which a ground state atom initially present in the trap is not detected in a subsequent imaging pulse. Both infidelity and imaging-induced losses will limit the ability to image and rearrange large atomic arrays [5,6].

The experimental fluorescence histograms are well modeled as the sum of three distributions. The first peak is centered on the number of background photons N_0 , with area the empty-trap probability $P_0 \simeq 50\%$. A second peak represents events where an atom is present for the full duration of the imaging. It is centered on $N_0 + N_1$ where N_1 is the number of photons scattered by the atom. Its area is $P_1 \times P_{\text{survival}}$ where $P_1 = 1 - P_0$ is the probability to have *initially* one atom in the trap and P_{survival} is the probability that the atom survives imaging. The third contribution is a flat distribution that bridges the two peaks, visible in Fig. 2(d), that corresponds to the events where atoms are lost while they are being imaged [8]. Its area is $P_1 \times P_{\text{loss}}$, with $P_{\text{loss}} = 1 - P_{\text{survival}}$. We give more details on the exact form used to model the distributions in [32]. Adjusting this model to the observed histograms, we extract the parameters N_0 , N_1 , P_0 , P_{loss} and estimate the best threshold to maximize the imaging fidelity F (see [32]). All quantities above depend in general on every imaging parameter such as exposure, imaging intensity, and detuning, as well as tweezer power. We optimized them to have the highest imaging fidelity.

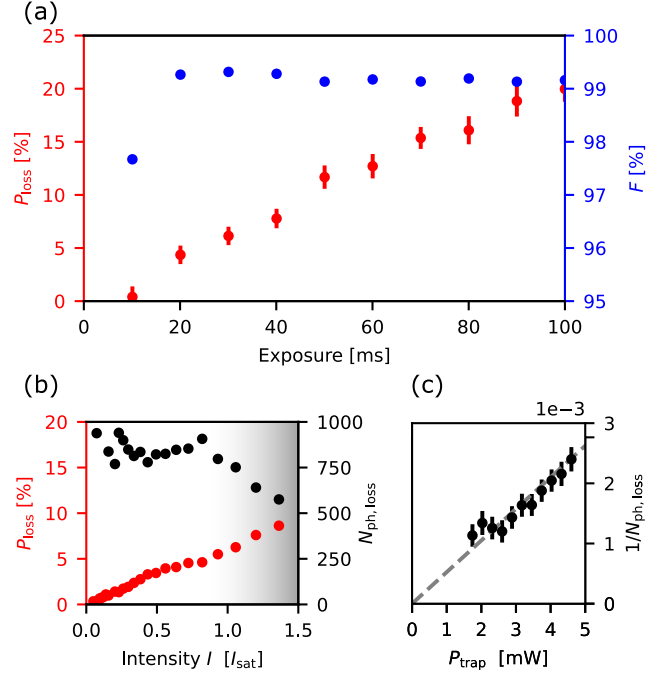


FIG. 3. (a) Imaging fidelity and loss probability as a function of the exposure time. (b) Loss probability (P_{loss}) and average number of 626 nm photons detected before a loss ($N_{\text{ph,loss}}$) as a function of imaging power for 30 ms exposure. In the shadowed area, losses are due to less efficient cooling. (c) The inverse of $N_{\text{ph,loss}}$ as a function of tweezer power. The dashed gray line is a linear fit.

For example, we show in Fig. 3(a) F and P_{loss} for several exposure times. At short duration, the fidelity is low because an atom does not scatter enough photons to be clearly distinguished from the background. The fidelity increases with exposure, eventually reaching a maximum after a few tens of milliseconds. However, the loss probability increases linearly with time. The imaging duration we choose is then a compromise between high fidelity and low losses. In typical conditions, we image the atoms in 30 ms, which is resilient to small fluctuations of parameters and we reach $F = 99.1(2)\%$ and $P_{\text{loss}} = 6.1(8)\%$ [40].

To identify the origin of the losses, we measured the influence of the imaging parameters on P_{loss} . We took a first picture to detect the atoms, then applied an imaging pulse for 30 ms varying the imaging parameters and finally measured the probability for the atom to have survived this pulse by taking a last image. The first and last pictures are taken with fixed parameters: 30 ms, $I = 0.8I_{\text{sat}}$, $\Delta = -\Gamma$. As shown in Fig. 3(b), we observe that P_{loss} increases linearly with imaging power. We also measure the average number of detected photons before an atom is lost $N_{\text{ph,loss}} = -N_{\text{detected}} / \ln(P_{\text{survival}})$ [41], where N_{detected} is the number of detected photons during the pulse. For $I \lesssim I_{\text{sat}}$, $N_{\text{ph,loss}}$ is approximately constant. It decreases for

higher intensities [gray area in Fig. 3(b)] due to less efficient Doppler cooling [42]. We also find that $N_{\text{ph,loss}}$ is constant when varying the detuning for $\Delta \lesssim -1 \Gamma$. Thus our observations suggest that the probability to lose an atom is directly proportional to the time it spends in the excited state $|e\rangle$.

This could be caused by a decay from $|e\rangle$ to dark or nontrapped states. However, the intercombination transition is closed and we have also checked that the atoms are not pumped to other Zeeman states of the ground manifold. These losses are thus likely due to further excitation by the trapping light from $|e\rangle$ to a highly excited state in Dy's dense spectrum. We indeed observe that the leakage to nonimaged states increases with trap power: Fig. 3(c) shows the inverse of $N_{\text{ph,loss}}$ for fixed imaging parameters as a function of trap power at 532 nm. A linear increase is observed showing that a deeper trap means a higher loss probability per imaging photon. We thus conclude that losses are due to a two-photon event: an atom in $|e\rangle$ absorbs a trap photon, sending it to a highly excited state from which it then decays to nonimaged states. There indeed exists a state with a dipole-allowed transition with $|e\rangle$ ($4f^{10}5d6p$, $J = 10$ at $34\,776.04 \text{ cm}^{-1}$) lying only about 400 GHz away from the sum of the two laser frequencies [43]. These losses are the main factor limiting imaging fidelity, and using a tunable trapping laser to increase the detuning from this state should allow to mitigate them. We expect this to be necessary for other lanthanides because of their dense spectrum.

We further observe that dark atoms can decay back to $|g\rangle$ from metastable states. Indeed, a trap initially containing an atom and that became dark sometimes spontaneously becomes bright again although the MOT is turned off. This can be seen on Fig. 4(a) where we plot the fluorescence of a single trap continuously imaged and observe discrete jumps from bright to dark and vice versa. Starting from initially empty traps, we do not observe the appearance of atoms, ruling out reloading from residual background pressure. Similar observations were reported with Yb in [10], identified as the excitation of the atom to metastable states and spontaneous decay to the ground state. To measure the average time it takes for the atoms to come back, we apply a pulse of imaging light for 1.5 s. After this pulse, about 70% of the atoms are no longer imaged. We plot in Fig. 4(b) the fraction of these dark atoms that subsequently reappear as a function of the wait time. We thus observe that 35% of them come back after a typical time $\tau = 0.48(8)$ s. From these measurements we extract a branching ratio of about 65% of decay toward trapped metastable states versus nontrapped ones [32]. We leave for future research the exact identification of these states.

We finally measured the temperature and lifetime of atoms in the tweezers. The lifetime in particular is important in views of sorting atoms to form large ordered arrays [44].

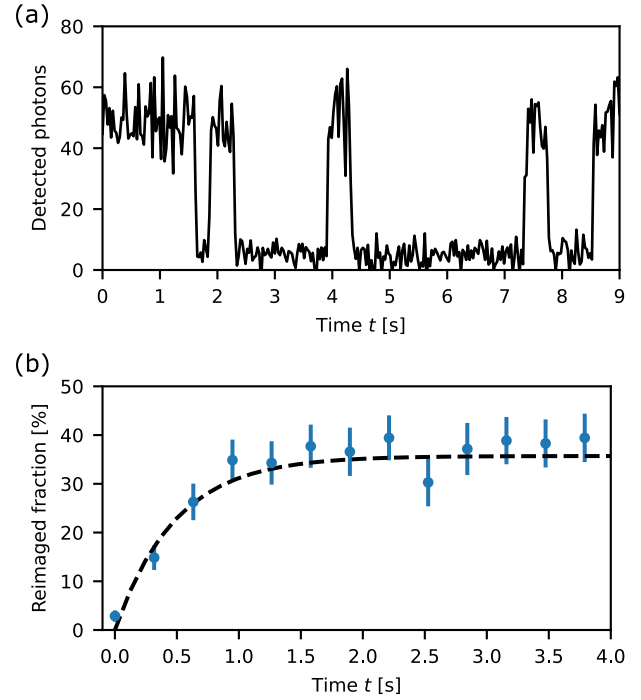


FIG. 4. (a) Number of collected photons over 30 ms for a given trap under continuous illumination but with no background gas to reload the trap. This shows events where the atom is pumped to metastable states and events where it decays back to the ground state. (b) Probability to reimagine an atom that previously became dark after having applied an imaging pulse of 1.5 s. The dashed line is a fit to an exponential saturation, with decay time $0.48(8)$ s.

For this, we used the release and recapture method; see [32]. Directly after imaging, we measured a temperature of $6.3(2) \mu\text{K}$, slightly higher than the Doppler temperature for the intercombination transition ($T_D = 3.2 \mu\text{K}$). Next, in shallow tweezers (depth $U_0 = 150 \mu\text{K}$, $P_{\text{trap}} = 2 \text{ mW}$), we observed a heating rate of $1.7(2) \mu\text{Ks}^{-1}$, that limits the lifetime in the absence of cooling to about 10 s. This heating rate is compatible with the off-resonant scattering of trap photons in the ground state. Indeed from the calculated imaginary part of the polarizability at 532 nm [45], we expect a heating rate of a few microkelvins per second. We mitigated this heating by applying cooling light (intensity $I = 5 \times 10^{-3} I_{\text{sat}}$, detuning $\Delta = -1.3 \Gamma$), and observed a lifetime of $300(30)$ s, limited by the two-photon losses studied above (see [32]).

In conclusion, we have demonstrated single-atom trapping and high-fidelity imaging of Dy on the intercombination line in tweezers rendered magic by fine tuning the tweezer polarization. Single-atom trapping of lanthanides opens exciting opportunities. For instance it can be used to obtain subwavelength distances using the anisotropic polarizability [18] or also by directly loading an accordion lattice. This could be used to create atomic waveguides [46], or to prepare directly extended Bose-Hubbard models [47] from optical tweezers.

We acknowledge fruitful discussions with Maxence Lepers and Jeff Thompson, experimental assistance by Florence Nogrette, and critical reading of the manuscript by Thierry Lahaye and Giovanni Ferioli. We note that another setup based on a similar 421-nm 2D-MOT loading a 626-nm 3D-MOT of Dy atoms has been developed in the group of L. Chomaz [37]. We have widely benefited from exchanges between our groups. This project has received funding by the Agence Nationale de la Recherche (JCJC grant DEAR, ANR-22-PETQ-0004 France 2030, project QuBitAF) and by the European Union (ERC StG CORSAIR, 101039361, ERC AdG ATARAXIA 101018511).

*Corresponding author: damien.bloch@institutoptique.fr

†Corresponding author: igor.ferrier-barbut@institutoptique.fr

‡Present address: Department of Physics, Stanford University, Stanford, California 94305, USA.

- [1] N. Schlosser, G. Reymond, I. Protsenko, and P. Grangier, Sub-poissonian loading of single atoms in a microscopic dipole trap, *Nature (London)* **411**, 1024 (2001).
- [2] F. Nogrette, H. Labuhn, S. Ravets, D. Barredo, L. Béguin, A. Vernier, T. Lahaye, and A. Browaeys, Single-atom trapping in holographic 2D arrays of microtraps with arbitrary geometries, *Phys. Rev. X* **4**, 021034 (2014).
- [3] A. Browaeys and T. Lahaye, Many-body physics with individually controlled Rydberg atoms, *Nat. Phys.* **16**, 132 (2020).
- [4] A. M. Kaufman and K.-K. Ni, Quantum science with optical tweezer arrays of ultracold atoms and molecules, *Nat. Phys.* **17**, 1324 (2021).
- [5] D. Barredo, S. de Léséleuc, V. Lienhard, T. Lahaye, and A. Browaeys, An atom-by-atom assembler of defect-free arbitrary two-dimensional atomic arrays, *Science* **354**, 1021 (2016).
- [6] M. Endres, H. Bernien, A. Keesling, H. Levine, E. R. Anschuetz, A. Krajenbrink, C. Senko, V. Vuletic, M. Greiner, and M. D. Lukin, Atom-by-atom assembly of defect-free one-dimensional cold atom arrays, *Science* **354**, 1024 (2016).
- [7] H. Kim, W. Lee, H.-g. Lee, H. Jo, Y. Song, and J. Ahn, In situ single-atom array synthesis using dynamic holographic optical tweezers, *Nat. Commun.* **7**, 13317 (2016).
- [8] A. Cooper, J. P. Covey, I. S. Madjarov, S. G. Porsev, M. S. Safronova, and M. Endres, Alkaline-earth atoms in optical tweezers, *Phys. Rev. X* **8**, 041055 (2018).
- [9] M. A. Norcia, A. W. Young, and A. M. Kaufman, Microscopic control and detection of ultracold strontium in optical-tweezer arrays, *Phys. Rev. X* **8**, 041054 (2018).
- [10] S. Saskin, J. T. Wilson, B. Grinkemeyer, and J. D. Thompson, Narrow-line cooling and imaging of ytterbium atoms in an optical tweezer array, *Phys. Rev. Lett.* **122**, 143002 (2019).
- [11] L. Anderegg, L. W. Cheuk, Y. Bao, S. Burchesky, W. Ketterle, K.-K. Ni, and J. M. Doyle, An optical tweezer array of ultracold molecules, *Science* **365**, 1156 (2019).
- [12] L. Chomaz, I. Ferrier-Barbut, F. Ferlaino, B. Laburthe-Tolra, B. L. Lev, and T. Pfau, Dipolar physics: A review of experiments with magnetic quantum gases, *Rep. Prog. Phys.* **86**, 026401 (2022).
- [13] N. Q. Burdick, Y. Tang, and B. L. Lev, Long-lived spin-orbit-coupled degenerate dipolar Fermi gas, *Phys. Rev. X* **6**, 031022 (2016).
- [14] T. Chalopin, T. Satoor, A. Evrard, V. Makhalov, J. Dalibard, R. Lopes, and S. Nascimbene, Probing chiral edge dynamics and bulk topology of a synthetic Hall system, *Nat. Phys.* **16**, 1017 (2020).
- [15] J. H. Becher, S. Baier, K. Aikawa, M. Lepers, J.-F. Wyart, O. Dulieu, and F. Ferlaino, Anisotropic polarizability of erbium atoms, *Phys. Rev. A* **97**, 012509 (2018).
- [16] T. Chalopin, V. Makhalov, C. Bouazza, A. Evrard, A. Barker, M. Lepers, J.-F. m. c. Wyart, O. Dulieu, J. Dalibard, R. Lopes, and S. Nascimbene, Anisotropic light shift and magic polarization of the intercombination line of dysprosium atoms in a far-detuned dipole trap, *Phys. Rev. A* **98**, 040502(R) (2018).
- [17] S. Nascimbene, N. Goldman, N. R. Cooper, and J. Dalibard, Dynamic optical lattices of subwavelength spacing for ultracold atoms, *Phys. Rev. Lett.* **115**, 140401 (2015).
- [18] L. Du, P. Barral, M. Cantara, J. de Hond, Y.-K. Lu, and W. Ketterle, Atomic physics on a 50 nm scale: Realization of a bilayer system of dipolar atoms, [arXiv:2302.07209](https://arxiv.org/abs/2302.07209).
- [19] T. Chalopin, C. Bouazza, A. Evrard, V. Makhalov, D. Dreon, J. Dalibard, L. A. Sidorenkov, and S. Nascimbene, Quantum-enhanced sensing using non-classical spin states of a highly magnetic atom, *Nat. Commun.* **9**, 4955 (2018).
- [20] A. Frisch, M. Mark, K. Aikawa, S. Baier, R. Grimm, A. Petrov, S. Kotochigova, G. Quéméner, M. Lepers, O. Dulieu, and F. Ferlaino, Ultracold dipolar molecules composed of strongly magnetic atoms, *Phys. Rev. Lett.* **115**, 203201 (2015).
- [21] T. Maier, I. Ferrier-Barbut, H. Kadau, M. Schmitt, M. Wenzel, C. Wink, T. Pfau, K. Jachymski, and P. S. Julienne, Broad universal Feshbach resonances in the chaotic spectrum of dysprosium atoms, *Phys. Rev. A* **92**, 060702(R) (2015).
- [22] M. Lepers, H. Li, J.-F. Wyart, G. Quéméner, and O. Dulieu, Ultracold rare-earth magnetic atoms with an electric dipole moment, *Phys. Rev. Lett.* **121**, 063201 (2018).
- [23] G. Anich, R. Grimm, and E. Kirilov, Comprehensive characterization of a state-of-the-art apparatus for cold electromagnetic dysprosium dipoles, [arXiv:2304.12844](https://arxiv.org/abs/2304.12844).
- [24] A. de Paz, A. Sharma, A. Chotia, E. Maréchal, J. H. Huckans, P. Pedri, L. Santos, O. Gorceix, L. Vernac, and B. Laburthe-Tolra, Nonequilibrium quantum magnetism in a dipolar lattice gas, *Phys. Rev. Lett.* **111**, 185305 (2013).
- [25] R. J. Bettles, S. A. Gardiner, and C. S. Adams, Enhanced optical cross section via collective coupling of atomic dipoles in a 2D array, *Phys. Rev. Lett.* **116**, 103602 (2016).
- [26] E. Shahmoon, D. S. Wild, M. D. Lukin, and S. F. Yelin, Cooperative resonances in light scattering from two-dimensional atomic arrays, *Phys. Rev. Lett.* **118**, 113601 (2017).
- [27] J. Rui, D. Wei, A. Rubio-Abadal, S. Hollerith, J. Zeiher, D. M. Stamper-Kurn, C. Gross, and I. Bloch, A subradiant optical mirror formed by a single structured atomic layer, *Nature (London)* **583**, 369 (2020).

- [28] T. Maier, H. Kadau, M. Schmitt, A. Griesmaier, and T. Pfau, Narrow-line magneto-optical trap for dysprosium atoms, *Opt. Lett.* **39**, 3138 (2014).
- [29] D. Dreon, L. A. Sidorenkov, C. Bouazza, W. Maineult, J. Dalibard, and S. Nascimbene, Optical cooling and trapping of highly magnetic atoms: The benefits of a spontaneous spin polarization, *J. Phys. B* **50**, 065005 (2017).
- [30] H. Kim, H. S. Han, and D. Cho, Magic polarization for optical trapping of atoms without Stark-induced dephasing, *Phys. Rev. Lett.* **111**, 243004 (2013).
- [31] The trapping laser is a Coherent Verdi V10 with measured wavelength 532.208 nm.
- [32] See Supplemental Material at <http://link.aps.org/supplemental/10.1103/PhysRevLett.131.203401> for a description of experimental techniques, which includes Refs. [33,34].
- [33] S. H. Youn, M. Lu, U. Ray, and B. L. Lev, Dysprosium magneto-optical traps, *Phys. Rev. A* **82**, 043425 (2010).
- [34] C. Tuchendler, A. M. Lance, A. Browaeys, Y. R. P. Sortais, and P. Grangier, Energy distribution and cooling of a single atom in an optical tweezer, *Phys. Rev. A* **78**, 033425 (2008).
- [35] The waist is defined as the $1/e^2$ radius of a Gaussian beam that fits best the expected radial intensity profile.
- [36] D. Bloch *et al.* (to be published).
- [37] S. Jin, J. Gao, K. Chandrashekhara, C. Götzhäuser, J. Schöner, and L. Chomaz, A 2D MOT of dysprosium atoms as a compact source for efficient loading of a narrow-line 3D MOT, *Phys. Rev. A* **108**, 023719 (2023).
- [38] J. Lee, J. H. Lee, J. Noh, and J. Mun, Core-shell magneto-optical trap for alkaline-earth-metal-like atoms, *Phys. Rev. A* **91**, 053405 (2015).
- [39] S. Ma, A. P. Burgers, G. Liu, J. Wilson, B. Zhang, and J. D. Thompson, Universal gate operations on nuclear spin qubits in an optical tweezer array of ^{171}Yb atoms, *Phys. Rev. X* **12**, 021028 (2022).
- [40] This means that out of the 6% of atoms that are lost during the imaging, most (roughly 5 in 6) are correctly labeled before being lost.
- [41] This comes from $P_{\text{survival}}(t) = e^{-t/\tau_{\text{loss}}} = e^{-N_{\text{detected}}/N_{\text{ph,loss}}}$.
- [42] P. D. Lett, W. D. Phillips, S. L. Rolston, C. E. Tanner, R. N. Watts, and C. I. Westbrook, Optical molasses, *J. Opt. Soc. Am. B* **6**, 2084 (1989).
- [43] W. C. Martin, R. Zalubas, and L. Hagan, Atomic energy levels: The rare earth elements, Technical Report, National Bureau of Standards, 1978.
- [44] K.-N. Schymik, B. Ximenez, E. Bloch, D. Dreon, A. Signoles, F. Nogrette, D. Barredo, A. Browaeys, and T. Lahaye, In situ equalization of single-atom loading in large-scale optical tweezer arrays, *Phys. Rev. A* **106**, 022611 (2022).
- [45] H. Li, J.-F. Wyart, O. Dulieu, S. Nascimbène, and M. Lepers, Optical trapping of ultracold dysprosium atoms: Transition probabilities, dynamic dipole polarizabilities and van der Waals c_6 coefficients, *J. Phys. B* **50**, 014005 (2016).
- [46] A. Asenjo-Garcia, M. Moreno-Cardoner, A. Albrecht, H. J. Kimble, and D. E. Chang, Exponential improvement in photon storage fidelities using subradiance and “selective radiance” in atomic arrays, *Phys. Rev. X* **7**, 031024 (2017).
- [47] L. Su, A. Douglas, M. Szurek, R. Groth, S. F. Ozturk, A. Krahn, A. H. Hébert, G. A. Phelps, S. Ebadi, S. Dickerson, F. Ferlaino, O. Marković, and M. Greiner, Dipolar quantum solids emerging in a hubbard quantum simulator, [arXiv: 2306.00888](https://arxiv.org/abs/2306.00888).